Darkening of interwell excitons in coupled quantum wells due to a stress-induced direct-to-indirect transition

J. K. Wuenschell,* N. W. Sinclair,† Z. Vörös,‡ and D. W. Snoke
Department of Physics and Astronomy, University of Pittsburgh, Pittsburgh, Pennsylvania 15260, USA

L. N. Pfeiffer and K. W. West
Department of Electrical Engineering, Princeton University, Princeton, New Jersey 08544, USA
(Received 28 March 2015; revised manuscript received 5 October 2015; published 9 December 2015)

In previous studies, an inhomogeneous strain field was used as a trapping mechanism for interwell excitons in coupled GaAs/$Al_{0.45}Ga_{0.55}$As quantum wells. Photoluminescence measurements in this system demonstrated the presence of a dark population of excitons at trap center in the low-temperature, high-stress, high-density regime. The dramatic appearance of this effect at low temperature and high density initially suggested that it may be indicative of a Bose-Einstein condensation phase transition. Further experiments revealed that this effect appears more readily in wider quantum wells and occurs at strain values near the heavy-hole/light-hole crossover point. In this paper, it will be shown that this effect occurs in a regime where the heavy-hole valence band maximum shifts away from $k_{||} = 0$, which is expected to strongly suppress the recombination rate at low temperatures. Simulations based on this assumption will be shown to match the experimentally observed behavior, without requiring the appearance of a Bose-Einstein condensate.

DOI: 10.1103/PhysRevB.92.235415 PACS number(s): 78.67.De, 73.21.Fg

I. INTRODUCTION

For many years, interwell excitons in coupled quantum wells have been a subject of intense study in the search for Bose-Einstein condensation in excitonic systems. While many signatures of Bose-Einstein condensation were observed in the microcavity exciton-polariton system as early as 2007 [1–3], interwell excitons remain interesting for several reasons. The spatial separation of electrons and holes that make up interwell excitons leads to a significantly longer radiative lifetime [4], providing much more time for the excitons to settle into spatial equilibrium in a trapping potential [5]. Interwell excitons also exhibit a long-range repulsive interaction characteristic of aligned electric dipoles [6,7], which suggests that the ground state might look much different than the ground state of microcavity polaritons.

Due to the density-dependent blueshift associated with the repulsion of interwell excitons, it is necessary to establish a trapping potential to achieve high density. Interwell excitons are characterized by a strong Stark shift in the presence of an electric field in the growth direction [8]. This allows electrostatic trapping methods [9–11], as well as accumulation of interwell excitons at the interface of cold electron and hole gases; measurements in this type of system have suggested the appearance of coherence of dipolar excitons at low temperature (in the 100 mK range) [12–14]. In response to [12], Semkat *et al.* [15] have argued that under similar (but not identical) numerically simulated conditions, it is possible to observe comparable fringe visibility entirely due to the optics of the point-spread function of a tiny exciton cloud. Subsequent high-resolution coherence measurements of trapped interwell excitons by Repp *et al.* [16] did not reveal any indication of spatial coherence at 250 mK, beyond that caused by the optical point-spread function. However, the degree to which these two reports can be directly compared to the aforementioned positive results is controversial.

Trapping of excitons using a spatially inhomogeneous strain is a technique that has been used in bulk semiconductors [17,18], microcavity polaritons [19], and coupled quantum well systems [20]. In the coupled quantum well system, it has been shown that strain trapping can produce a high-density population of interwell excitons in equilibrium [21].

This paper addresses an effect in which the recombination rate of a population of indirect excitons is sharply suppressed due to an applied stress; it will be shown that this can be explained by a strain-induced transition where the band gap becomes slightly momentum-space indirect. This effect was observed in strain trapped interwell excitons in 14-nm and 12-nm coupled quantum wells separated by a 4-nm barrier in a GaAs/$Al_{0.45}Ga_{0.55}$As structure. In this system, a spatially inhomogeneous strain trap was formed by using a stainless steel pin to stress a 100-μm thick, 5 mm $\times$ 5 mm chip clamped on top of a 1-mm radius hole in a metal plate (see Fig. 1). This geometry was shown in previous work to produce a nearly harmonic trap directly underneath the pin, with a maximum trap depth of around 20–30 meV (limited by fracture of the sample).

It was observed that in an intermediate stress range (typically 3–5 meV for 14-nm wells), a dark region in the luminescence at the interwell exciton energy would appear at the center of the trapped population. Analysis of the luminescence linewidth suggested that this region was associated with a suppressed radiative rate, rather than a depletion of excitons [22]. The effect occurred only at low temperature (with a typical onset below 10 K) and disappeared at low exciton density. The temperature and density dependence were suggestive of Bose-Einstein condensation (BEC), particularly in the light of theoretical predictions of condensation in dark

*jkwuenschell@gmail.com
†Current address: Institute for Shock Physics, Washington State University.
‡Current address: University of Innsbruck; zvoros@uibc.ac.at

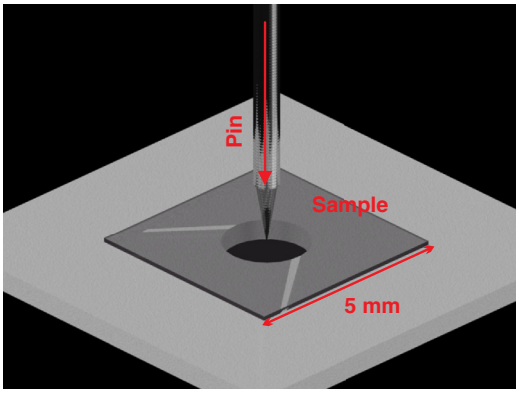

FIG. 1. (Color online) Diagram of the stressor geometry. The sample (a 5 mm × 5 mm chip) sits on a metal plate on top of a 1 mm radius hole and is stressed with a micrometer-driven pin, typically with 50 μm tip radius or less, centered over the top of the hole.

states [23] or partially dark states [24]. Other experimental works which do not utilize strain-based traps have attributed the appearance of a dark population as a sign of BEC [14,25].

Comparison between systems with 12-nm and 14-nm quantum wells revealed that the effect occurred at lower stress with 14-nm quantum wells. It was also observed that at high stress, the system goes into another regime in which a bright spot appears in the luminescence at trap center. Spectrally resolving this luminescence revealed a second energy line poking through the ground state at high stress. This was interpreted as the light-hole exciton passing through the heavy-hole exciton (which is the ground state at zero stress) [22]. This behavior suggested that the effect may be related to strain-induced band mixing of the heavy- and light-hole exciton states.

In Sinclair *et al.* [22], band mixing was proposed as a possible explanation for this effect, relying on the fact that the light-hole interwell exciton is expected to have a faster recombination rate than the heavy-hole exciton, due to the greater penetration of the light hole into the quantum well barrier. It was shown that the trapping potential is expected to induce a small amount of mixing between heavy-hole and light-hole states; this was supported by polarization measurements which agreed with the prediction of the mixing theory. It was also shown that this could cause a relative brightening at the sides of the trap, which might make the center of the population look dark by comparison. While simulations using this model predicted an onset of the darkening effect at a critical stress consistent with the experiments, they did not explain the temperature dependence of this effect, and they predicted a sharp decrease in the population lifetime at this critical stress which was not observed experimentally.

In this work, we show through calculations of the stress-dependent band structure that a momentum-space direct-to-indirect transition is expected at a critical stress in this system. Using a simple model to determine the expected effect of this transition on the photoluminescence profile, we show that a strong suppression of the luminescence at trap center is expected. We will also show that the stress dependence, density dependence, and temperature dependence of this effect are all explained by this interpretation, and that it also is consistent with the time-resolved photoluminescence measurements. This behavior is not unlike that of interwell excitons in an in-plane magnetic field, which shifts the exciton energy minimum away from $k_{||} = 0$; a suppressed radiative rate caused by a direct-to-indirect transition in a magnetic field was observed by Butov *et al.* [26].

This work will deal with excitons that are both spatially indirect (with the electron and hole sitting in different wells, due to the applied electric field) and, in some regimes, momentum-space indirect. To avoid confusion, spatially direct exciton states will be referred to as DX or intrawell, and spatially indirect states will be referred to as IX or interwell.

II. EXPERIMENTAL FEATURES

Creating interwell excitons with resonant absorption can be very inefficient, because the absorption efficiency is inversely proportional to the radiative lifetime. An alternative approach is to resonantly excite intrawell excitons, which can then relax to the interwell state via carrier tunneling across the coupled quantum well barrier. The tunneling rate across the barrier in the system under discussion is sufficient (compared to the DX radiative recombination rate) for a significant fraction of the excited population to relax into the interwell state. The energy splitting between the DX and IX states also makes it easy to spectrally filter out the scattered laser light and isolate the IX photoluminescence.

The excitation source used in these experiments was a laser diode with a Peltier cooler, which provided a tunable wavelength near-resonant to the DX line (which typically sits near 808 nm in 12-nm quantum wells). Interwell excitons were introduced into the system by pumping the direct line with cw or quasi-cw illumination. Intrawell excitons are generated by the laser pulse, then quickly relax down the interwell ground state within 1 μs.

The behavior of the interwell exciton population was analyzed by collecting the photoluminescence (PL) emitted from the sample and reimaging it onto an intensified CCD (ICCD) camera. Some of the results shown here are 2D spatial profiles observed by directly reimaging the PL onto the ICCD. Spectrally resolved PL data are also shown, which are gathered by collecting a spatial cross section of a magnified image of the exciton cloud along a 100 μm slit, then passing that luminescence through a spectrometer with a 1200 mm^{-1} grating with 750 nm blaze.

The most striking feature of the high-stress, high-density regime is the dramatic appearance of a dark population at trap center. In Fig. 2(a), the stress dependence of the photoluminescence 2D spatial profile is shown for a 12-nm coupled quantum well sample. In this series, the sample was illuminated with a cw laser at approximately 120 μW average power, 4 meV above the the direct line and focused on the center of the trap. The DX luminescence and scattered laser light were removed by an 819-nm, 10-nm FWHM bandpass filter [27]. The sample was held at low temperature (2.2 K) in a continuous-flow cryostat and an additional voltage drop of 0.5 V was applied in the same direction as the built-in field due the *p-i-n* doping.

The initial experimental results were performed for 12-nm coupled quantum wells with a 4-nm $Al_{0.45}Ga_{0.55}As$ barrier. The

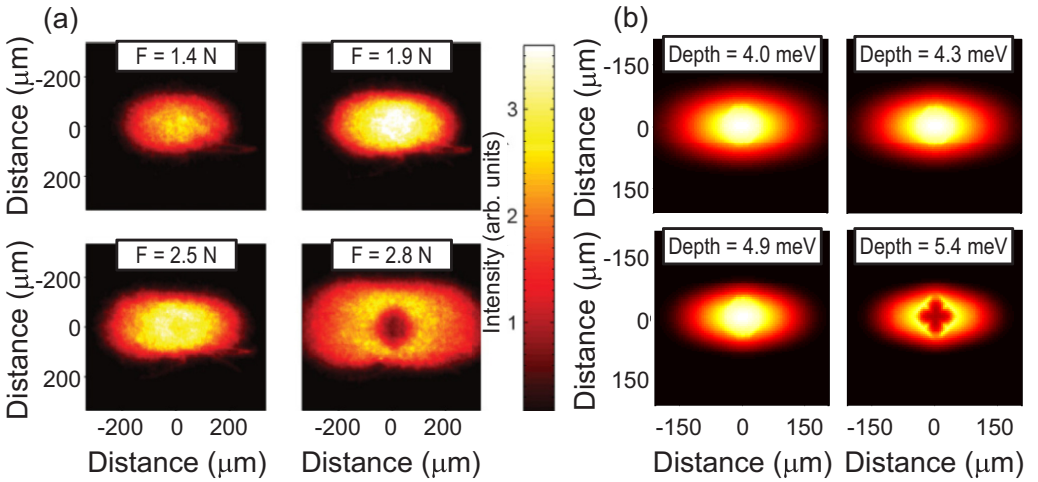

FIG. 2. (Color online) Comparison of (a) experimentally measured 2D spatial profiles of the photoluminescence from 12-nm CQWs as a function of stress (from Sinclair *et al.* [22]) and (b) a similar series of 2D spatial profiles of the intensity calculated using the model discussed in Sec. III. Both images correspond to a temperature of approximately 2 K. The experimental data are taken at fixed pump power; this is approximately captured in the model by fixing the density at trap center.

effect is similar in a system with 14-nm quantum wells, but occurs at lower stress. This dependence on the well width is a critical clue to the origin of this behavior: the darkening occurs in the stress regime near where the lh-exciton line crosses over the hh-exciton line. For narrower wells, the hh-lh splitting is larger, and this regime occurs at higher stress.

Figure 3(a) shows that the luminescence from 12-nm coupled quantum wells (CQWs) at trap center darkens significantly and sharply as the temperature drops from 9 K to 4 K at a fixed stress. This series shows the two-dimensional profile of the luminescence at fixed pump power (50 μW). The DX luminescence is removed by a bandpass filter, as with the stress series. It is worth noting that the size of the dark spot does not seem to grow as temperature drops—instead, the brightness relative to the trap periphery drops as temperature decreases.

It was also observed that the dark spot decreases in size as optical pump power is decreased, although it does not sharply appear or disappear with varying pump power, as it does with temperature and applied stress. In Fig. 4(a), a spatial cross section of the photoluminescence intensity through the center of the trap is shown as a function of average pump power. For this data set, 12-nm CQW samples were used. The matching 2D spatial profiles are shown in Fig. 4(b). In this series, the excitation source was gated such that the pulse was on for 2 μs and off for 6 μs; the ICCD was gated such that the excitation pulse was eliminated from the exposure (the exposure starts 200 ns after the pulse ends and ends 100 ns before the next pulse begins). The measurement was performed at fixed stress and temperature (1.8 K). As with previous results, a bandpass filter was used to eliminate any residual light not associated with the interwell excitons. The general trend that can be observed in

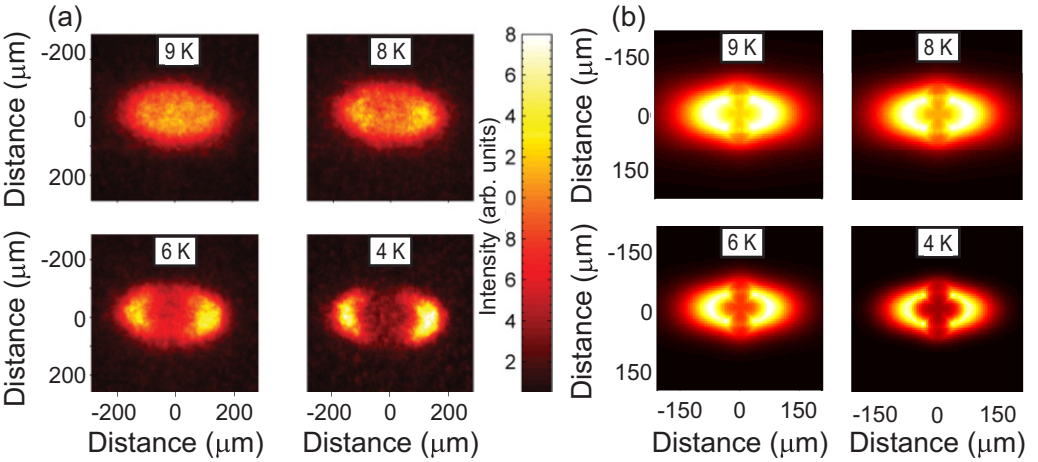

FIG. 3. (Color online) Comparison between (a) experimentally measured, 2D spatial profiles of the photoluminescence from 12-nm CQWs as a function of temperature (from Sinclair *et al.* [22]) and (b) a similar series of 2D spatial profiles of the intensity calculated using the model discussed in Sec. III. In (a), as in [22], the profiles are parametrized by the applied force on the pin; in (b), the profiles are parametrized by the total depth of the trapping potential.

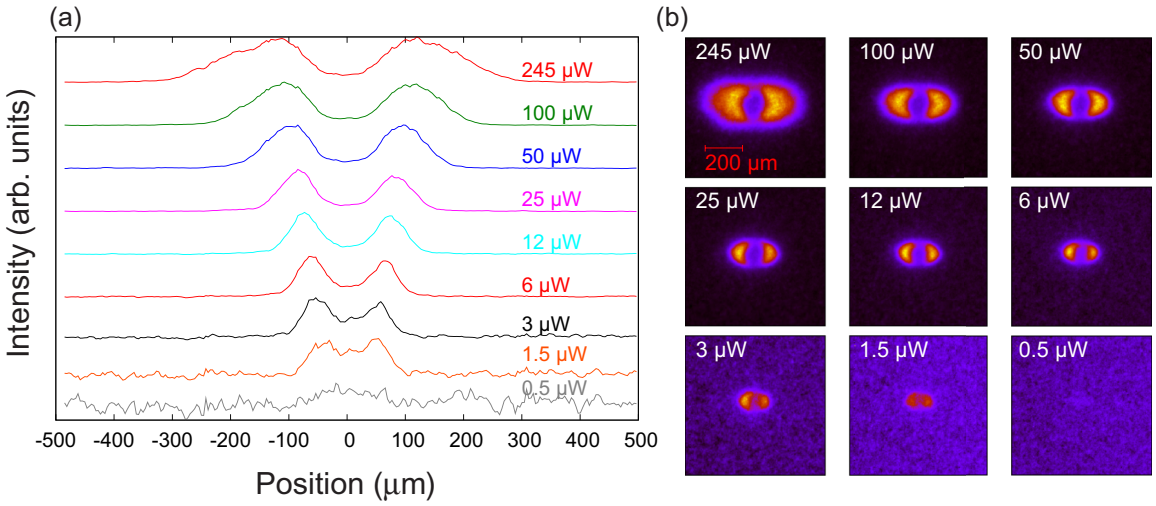

FIG. 4. (Color online) Gated interwell exciton photoluminescence from 12-nm CQWs at a fixed stress within the stress and temperature regime where the dark region is visible. The sample temperature is fixed at 1.8 K and the optical pump power is varied. (a) Spatial cross section of the intensity through the weak confinement axis. (b) 2D spatial profile of the intensity, with the color scale displaying intensity in arbitrary units.

Figs. 4(a) and 4(b) is that, while there is no sharp onset of the dark spot with power, it does shrink as the size of the exciton cloud decreases.

A careful analysis of the IX population decay dynamics as a function of stress also confirms that there is an overall drop in the local radiative rate at trap center. The population lifetime was measured by integrating the collected photoluminescence from the IX population over 5 μs time windows, starting from a range of delay times after the excitation pulse, as shown in Fig. 5(a). In this text, the population lifetime is associated with the rate at which the entire trapped IX population decays into photons. The time scale at which the IX population spatially distributes itself within the trapping potential is small compared to the lifetime, so it is assumed that the population is approximately in spatial equilibrium at all times (this assumption will be discussed further in Sec. III). In the event of a spatially varying radiative rate, the population lifetime would be associated with a spatial average of the local radiative rate across the trapping potential, weighted by the local density at each point.

As seen in Fig. 5(a), at low stress the entire IX population is accurately modeled by a single-exponential decay rate, with a fitted time constant [plotted in Fig. 5(b)] of around 15 μs. After the dark spot onset, it more closely matches a model with two different single-exponential decays: a fast decay rate which dominates at early times and a slower (approximately 2 to 3 times slower) rate which dominates at late times. Figure 5(b) illustrates that at a critical stress value coinciding with the appearance of the dark region, the dominant decay rate at late times (between 30 and 90 μs after the excitation source is cut off) becomes drastically different from the decay rate observed at earlier times.

At early times, when the interwell exciton population in the trap is largest, the exciton cloud will be more spread out across the trap profile due to dipole repulsion [quantified by the

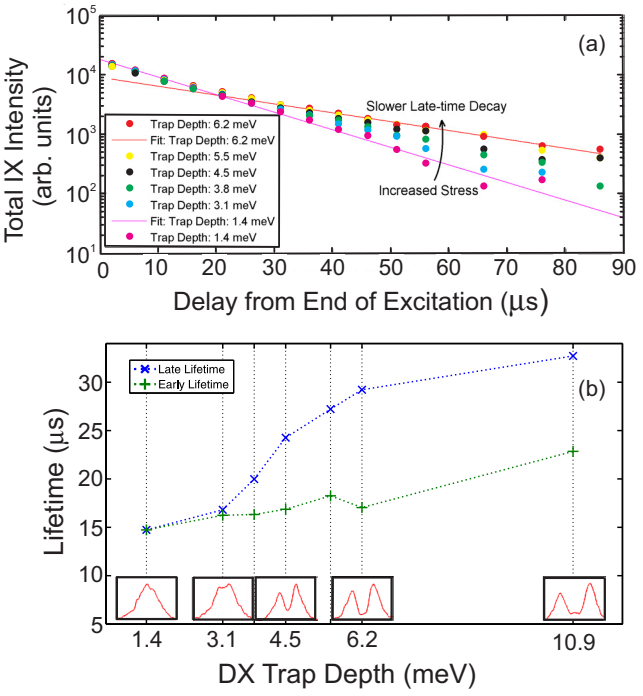

FIG. 5. (Color online) Single-exponential fit of population lifetime vs DX trap depth at early and late times in the 12-nm CQW sample, normalized with respect to the intensity directly after the pulse at each stress value. The intensity emitted by the entire trapped IX population was integrated over 5 μs windows as a function of delay time from the end of the excitation pulse; in (a), these measurements were plotted over a range of stress values, parametrized by the trap depth. The decay constants were fitted for delay times 0–25 μs after the pulse (early lifetime) and delay times 30–90 μs after the pulse (late lifetime), and plotted in (b). The insets in (b) show the time-integrated spatial profile of the intensity for several strain values.

density-dependent blueshift in Eq. (2)]. At late times, when the average density is lower, the population will be more localized towards the center of the trap. A nearly constant decay rate—as observed in Fig. 5(a)—indicates that the radiative rate does not vary significantly across the trapping potential in that stress regime. In the stress regime where the dark spot is visible, the time dependence of the population lifetime, observed in Fig. 5(b), is consistent with an enhanced local lifetime (and, hence, a lower radiative rate) in the dark, central region.

III. DIRECT-TO-INDIRECT TRANSITION

In a theoretical study of 10-nm GaAs/$Al_{0.21}Ga_{0.79}As$ quantum wells by Andreani *et al.* [28], it was shown that for a compressive uniaxial stress a maximum in the highest valence subband can appear away from $k_{||} = 0$, where $k_{||}$ corresponds to the component of the momentum parallel to the plane of the quantum wells, near the hh-lh crossover point. This occurs due to intersubband mixing at finite $k_{||}$ and results in an indirect gap. In indirect-gap semiconductors, recombination is strongly suppressed due to the k-space separation between electrons and holes; in these systems, recombination generally requires a slow, phonon-assisted process to conserve momentum [29].

The valence band dispersion relationship in our coupled quantum well structure was calculated by diagonalizing the summed Luttinger-Kohn and Pikus-Bir Hamiltonians [30] superimposed on a 1D position basis along the growth direction. The strain components inserted into the Pikus-Bir Hamiltonian were found using ANSYS, a finite-element software package. A plot of the two lowest calculated exciton energy states for 12-nm CQWs at $k_{||} = 0$ is shown in Fig. 6 as a function of applied force. The hh-lh crossover point occurs around the nominal force value of 1.5 N in the calculation. Note that it is difficult to directly compare the experimental force values with the calculated force values, due to uncertainty in the actual contact area of the pin (due to surface roughness).

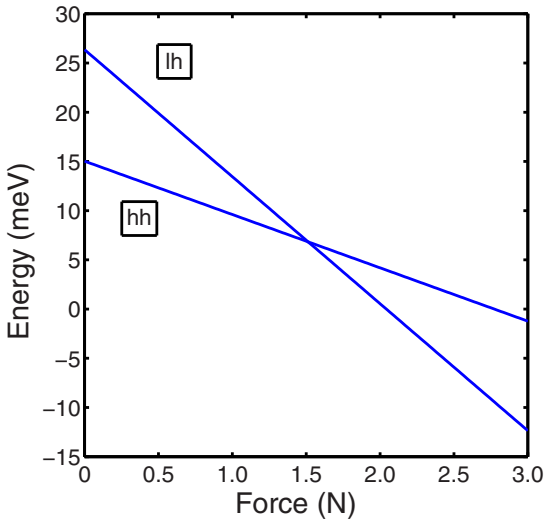

FIG. 6. (Color online) Calculated heavy- and light-hole exciton energies at trap center and $k_{||} = 0$ for 12-nm CQWs as a function of force, showing the crossover point at a nominal value of around 1.5 N. This calculation includes only the confinement energy and the shift due to strain. Recall that the exciton energy is equal to the difference between the conduction band minimum and valence band maximum, plus the binding energy. The binding energy is not included in this calculation, but is not expected to be significantly different for the two states or strongly stress-dependent.

A calculation of the 2D $k_{||}$ dependence of the highest valence band for 12-nm CQWs at this force value, shown in Fig. 7(a), illustrates that the valence band maxima occur at finite $k_{||}$ along the (110) and $(1\bar{1}0)$ axes. This behavior is shown in more detail in Fig. 8(a), where the gap between the valence band maximum and the valence band energy at $k_{||} = 0$ is plotted as a function of force. In Figs. 8(b)–8(e), a cross section of the dispersion curve along the (110) axis is shown at several different force values, illustrating the appearance of a valence band maximum at finite $k_{||}$ above $F = 1.1$ N [this can be seen at $F = 1.21$ N in Fig. 8(c)] and its disappearance when the light-hole state completely pokes through and becomes direct again, around $F = 2.4$ N [Fig. 8(e)].

Although the uppermost valence band appears to exhibit a local minimum at $k_{||} = 0$ near the hh-lh crossover point in Fig. 8(d) (at $F = 1.52$ N), the effective mass at very small $k_{||}$ is never observed to be negative. Instead, the point at $k_{||} = 0$ remains a shallow local maximum and the local minimum [visible in the plot for $F = 1.21$ N, Fig. 8(c)] moves closer to zero as the hh and lh bands approach each other. When they meet [around $F = 1.52$ N, Fig. 8(d)], band center briefly becomes a stationary inflection point before the local maximum reappears at higher stress [which is somewhat visible in the plot for $F = 2.40$ N, in Fig. 8(e)].

In addition to the process of the energy bands going from direct to indirect, the effective in-plane mass of the ground state also changes significantly during this process. It is reasonable to expect that the character of the ground state excitons in this system also changes in this regime. A rigorous treatment of this behavior would require calculating the ground state exciton wave function using the modified dispersion relationship. Performing this calculation as a function of strain and along a 2D spatial profile of the trap is computationally intensive. In our simulations we therefore start by ignoring this change of mass. The effect of the exciton mass varying with stress will be addressed in Sec. IV.

Typically, radiative recombination in indirect semiconductors occurs via a phonon-assisted process [29]. In this scenario, excitons are constructed out of electrons and holes that are significantly separated in k-space. In the case of AlAs, an indirect semiconductor, the conduction band energy at the Γ point is almost 1 eV higher than conduction band minimum [31], meaning that the conduction band states associated with direct recombination are virtually unoccupied at room temperature. Thus all recombination occurs between electrons and holes that have significantly different crystal momentum; this process must be phonon-assisted in order to satisfy energy and momentum conservation. In the present system, the direct and indirect gap states are separated by a few meV or less, compared to a thermal energy of around 0.17 meV at 2 K. While the occupation of direct gap states is expected to be suppressed, we expect that recombination via thermally excited momentum-space direct excitons is still a viable pathway for recombination. Given the long lifetime of interwell excitons, we can assume that the population of the

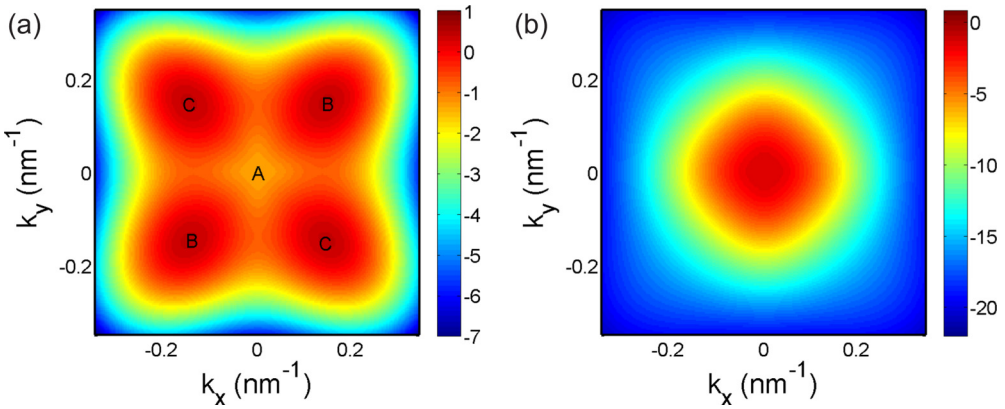

FIG. 7. (Color online) Calculated 2D $k_{||}$ dependence of the valence band energy for (a) the highest and (b) the second-highest valence subbands in 12-nm CQWs at the expected hh-lh crossover point ($F = 1.52$ N in Fig. 8). In the highest subband, the maxima clearly appear away from $k_{||} = 0$, along the (110) and (1$\bar{1}$0) axes. The five critical points are labeled as discussed in Sec. IV.

direct excitons is given by a Boltzmannian factor for thermal equilibrium.

One simple model to take this behavior into account is to assume that the radiative recombination rate is suppressed by the factor associated with thermal occupation of the direct states,

$$\frac{1}{\tau} = \frac{1}{\tau_0}\exp\left[-\frac{\Delta E_I}{k_B T}\right], \tag{1}$$

where τ_0^{-1} is the radiative rate for direct recombination and ΔE_I is the difference between the indirect band gap and the direct gap [as shown in the calculation of Fig. 8(a), this energy difference peaks at just under 2 meV]. This expression can be easily calculated for the strain distribution along the trap spatial profile. This approximation will be referred to as the "gap model."

Using the expression in (1), the intensity profile can be calculated as a function of stress (parametrized by the trap depth, defined as the calculated difference between the energy at trap center and the energy far away from the trap). In this calculation, a Boltzmann distribution with a linear density-dependent blueshift (with proportionality constant γ) is assumed [7]:

$$n(x,y) = n_0 \exp\left[-\frac{U(x,y)}{k_B T} - \frac{\gamma n(x,y)}{k_B T}\right], \tag{2}$$

where $U(x,y)$ is the potential energy due to the strain field felt by the excitons, and $n(x,y)$ is their local density. For 10-nm coupled quantum wells, careful experimental and theoretical analysis, by Vörös *et al.* [7] and Schindler *et al.* [32], respectively, suggest that the parameter γ should be in the range of 10^{-10} to 10^{-11} meV cm^2 [33]. Ultimately, the model below is parametrized entirely by the blueshift of of the population at trap center, which does not require precise, independent measurements of γ or the absolute density.

The density-dependent blueshift flattens out the trapping potential, forcing the population to spread out across the trap when the total trapped population is high. It also sets an upper limit to the total population in the trap; if the trapped population is too large, the renormalized trapping potential will be completely flattened out. The radiative intensity can be found using the calculated radiative rate of the ground state,

$$I(x,y) = \frac{n(x,y)}{\tau_{gs}(x,y)}. \tag{3}$$

If the trap energy $U(x,y)$ is defined such that the potential at trap center is equal to zero, the density can be conveniently parametrized by the blueshift at trap center, γn_0. Both (2) and (3) rely on the assumption that the time required for the exciton population to reach spatial equilibrium in the trap is short compared to the radiative lifetime. If this were not true, a more accurate model would need to take into account exciton transport from long-lifetime regions to short-lifetime regions. In practice, the density would accumulate in the long-lifetime regions and would be preferentially depleted in short-lifetime regions compared to the density profile given by (2). The effective lifetime observed in short-lifetime regions would also be increased, associated with the bottleneck of exciton transport into that region.

Interwell exciton equilibration was studied experimentally by Vörös *et al.* [5] in a similar system containing 10-nm coupled GaAs quantum wells separated by a 4 nm $Al_{0.3}Ga_{0.7}As$ barrier. It was shown that spatial equilibrium with a strain-based trapping potential was approximately reached in about 1 μs, which was less than the radiative lifetime for the system under consideration in Vörös' work (approximately 3.6 μs). This is also significantly less than the radiative lifetime of the system discussed here, which is in the range of 15–30 μs (see Fig. 5). This strongly suggests that the exciton population is very close to spatial equilibrium at all times and that Eqs. (2) and (3) are justified.

Figure 2(b) shows the 2D intensity profile at varying stress calculated in this way; in this series the temperature is fixed at 2 K ($k_B T = 0.17$ meV) and the total density is fixed such that the blueshift at trap center is 70% of the trap depth. In this model, a piezoelectric effect is included which elongates the trap along one direction, as is observed experimentally [22]. Other than the dependence given in (1), the radiative recombination rate is assumed to be independent of stress (changes in the in-plane mass or in the confinement direction are not taken into consideration). Suppression of the luminescence at trap center is observed at a critical stress

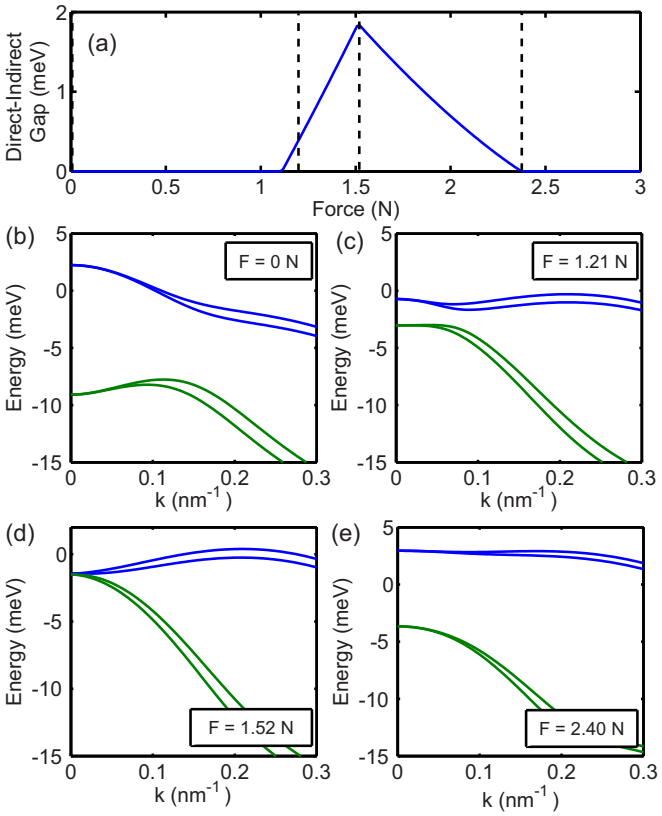

FIG. 8. (Color online) Valence band structure as a function of force at trap center for 12-nm coupled quantum wells in a 1 mV/nm electric field. Plot (a) shows the gap between the calculated valence band maximum and the valence band energy at $k_{||} = 0$, as a function of applied force on the stressor. The four lower subfigures show the heavy-hole (blue) and light-hole (green) valence subbands as a function of in-plane momentum along the (110) axis, at several different values of force. Below approximately 1.1 N, the valence band maximum is at $k_{||} = 0$, which corresponds to a gap of zero [shown for $F = 0$ N in (b)]. Above this force value, a gap opens up [as demonstrated at 1.21 N in (c)] and grows until the force reaches the value corresponding to the hh-lh crossing [around 1.5 N, shown in (d)]. Then the gap slowly closes, with the valence band maximum going back to $k_{||} = 0$ when the light-hole band fully passes through the heavy-hole band [the cusp of this is shown at $F = 2.4$ N in (e)].

value, producing a spatial intensity pattern very similar to the experimentally observed result in Fig. 2(a).

In the stress series, constraining the density blueshift at trap center in the simulation is not exactly the same as maintaining constant pump power. The absorption of the DX line, the DX-to-IX transition rate, and the radiative lifetime of the IX state will all vary with stress. This means that the population in the trap and the density at trap center are expected to change with stress. For example, it is clear that the size of the trapped exciton cloud increases with stress in the measured photoluminescence [Fig. 2(a)], but shrinks in the simulated result [Fig. 2(b)]. A more complicated treatment of the constant pump power constraint would result in a larger trapped population with increased stress (due to the increase in radiative lifetime). However, the key feature we wish to convey in Fig. 2 is that the dark population appears sharply with stress, a result which is captured perfectly by the model.

The shape of the dark spot in the model also does not exactly match the experimentally observed shape; that is, the above model predicts a clover pattern, where a more elliptical shape is observed experimentally. This could be due to a built-in ϵ_{xy} component of the strain; this component of the shear strain contributes to the hh-lh mixing within the Luttinger-Kohn model and has a quadrupolar spatial profile within our geometry. A small offset to this component of the strain would make this profile look more elliptical. It was also found that a small built-in offset to this component of the strain is necessary to explain a very slight spatial asymmetry of the direct luminescence spectral profile, not attributable to the piezoelectric effect [34].

In this model, the role of temperature is straightforward. When the average thermal energy is comparable to or larger than the gap between the valence band maximum and the direct recombination states, there will be substantial occupation of direct recombination states near $k_{||} = 0$ and there will not be significant suppression of the radiative rate. The temperature dependence of the intensity profile within this model is shown in Fig. 3(b), where the stress is fixed (at a bare trap depth of 5.8 meV) and the density is fixed such that the blueshift at trap center is 30% of the trap depth. At this force, a strongly contrasted dark region is observed at low temperature, but is brightened significantly at higher temperature ($T = 10$–18 K). This compares well with the experimentally observed temperature dependence presented in Fig. 3(a), where the dark region appears to disappear at around 9 K.

Note that the dark spot is still slightly visible at 9 K in the modeled images. The point where this feature disappears entirely will be strongly dependent on the applied force and, as one can see from Fig. 8(a), the onset temperature will vary with the direct-to-indirect gap; the onset temperature predicted by the model is expected to be less than 21 K (where 21 K corresponds to a thermal energy of around 1.8 meV).

The variation of population lifetime with stress, shown in Fig. 5, is also explained by the appearance of a k-space indirect region at trap center. At early times, the exciton cloud is spread over the entire trap and the overall decay rate will be dominated by excitons occupying the shorter-lifetime periphery of the trap. At late times, when the exciton cloud has contracted almost entirely into the dark region, the longer population lifetime will correspond to the longer local lifetime within this region.

IV. EFFECT OF EXCITON MASS

The approximation (1) qualitatively explains the stress and temperature dependence, but the power dependence of the dark spot shape is not as accurate. This can be seen in Fig. 9(b), where a cross section of the modeled PL intensity is shown as a function of density at fixed stress (6.3 meV bare trap depth) and temperature (4 K). Figure 9(b) illustrates that the gap model predicts a sharp spatial cutoff of the intensity between the high and low radiative rate regions with sharp, cusplike peaks. The intensity profile exhibits a local minimum at trap center; however it does not match up very well with the overall shape of the experimental result in Fig. 4(a). Specifically, the

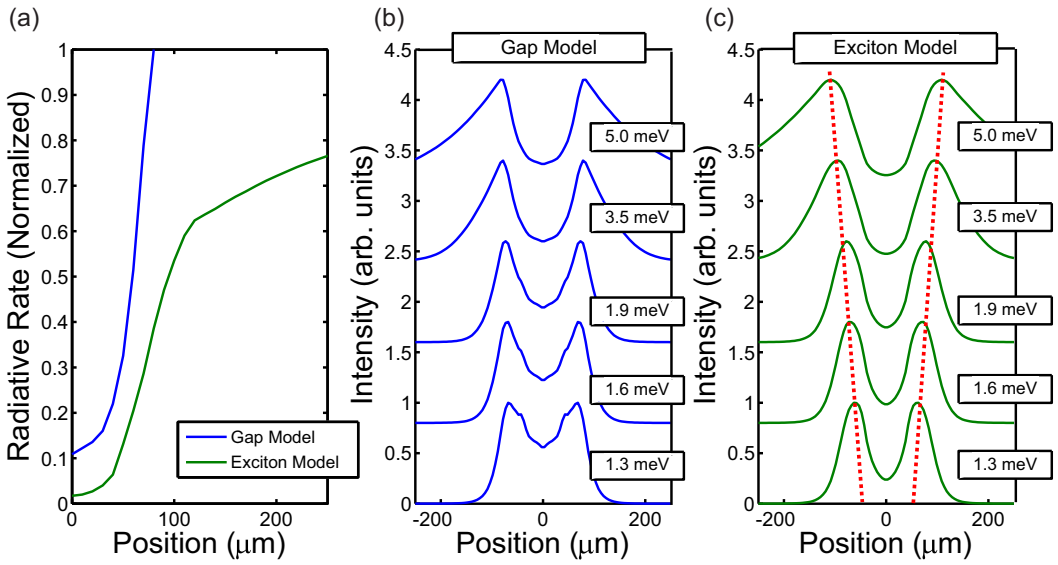

FIG. 9. (Color online) In (a), the radiative rate as a function of position along a cross section of the trap (in the [110] direction) is shown for the simple direct-indirect gap model and the exciton fit model, both for 12-nm quantum wells, as discussed in Sec. III and Sec. IV, respectively. Both are normalized such that the radiative rate goes to unity far away from the center of the trap. A plot of the calculated intensity through a cross section of the trap is shown in (b) for the direct-indirect gap model and (c) for the exciton fit model. The profiles shown are calculated for fixed stress (at a bare trap depth of 6.3 meV) and at a fixed temperature of 4 K. The inset energies correspond to the density, parametrized by the density-dependent blueshift at trap center. The red dotted lines in (c) approximately illustrate the increase in the size of the dark region with power. The plot in (c) can be compared to a similar experimental plot in Fig. 4(a).

modeled shapes of the peaks at the edge of the dark region are very sharp and do not move significantly with increased power.

Assuming a gradual spatial dependence of the radiative lifetime, one would expect the dark spot to widen with power; the location of the bright edge of the dark spot is determined by the tradeoff between the density distribution (which is peaked at the center of the trap, but widens with increased pump power) and the radiative rate (which is lowest at the center of the trap). For a sharp cutoff between the high and low radiative rate regions, as predicted within the gap model [as shown in the "gap model" curve in Fig. 9(a)], the edge of the dark spot should be roughly fixed at the boundary of the direct and indirect regions, which is fixed by the stress. In defining the bright and dark regions of the intensity profile, this sharp boundary overwhelms the gradual spatial variation of density, and causes the edge of the dark region to be relatively independent of trapped population [see Fig. 4(b)].

The gap model discussed in Sec. III only looks at the change in the critical points of the valence band with stress, rather than the exciton itself. It is expected that the conduction band will not change drastically with stress, apart from an overall hydrostatic shift. This approximation would be reasonable if we were looking at the recombination of free carriers. It would also be a reasonable approximation if the system were composed of two identical [35], coexisting exciton populations in equilibrium, with slightly different band gap energies.

A more accurate approach is to take the new valence band dispersion relationship into consideration to calculate the overall exciton dispersion relationship. Using the effective mass of each exciton state, one can then calculate the fraction of indirect excitons that are both radiatively active and able to emit within the collection angle of the imaging optics. To do this rigorously, it is necessary to calculate the exciton wave function including the Coulomb interaction between the electron and hole, taking the warped hole dispersion relationship into consideration at each stress point. A simpler way to calculate the exciton dispersion relationship is to treat each valence band maximum as a distinct hole state with its own effective mass. The effective mass can be found in the usual way, by fitting the minimum to a parabolic dispersion relationship:

$$E_{\text{hole}} = \frac{\hbar^2}{2m_{h,110}}k_{110}^2 + \frac{\hbar^2}{2m_{h,1\bar{1}0}}k_{1\bar{1}0}^2. \tag{4}$$

To account for the asymmetry of the maxima away from $k_{||} = 0$, the (100) and $(1\bar{1}0)$ directions will be the principal axes. The exciton mass is then given by the sum of the electron and hole masses, as follows:

$$m_{\text{ex}} = m_{\text{e}} + m_{\text{h}}(x, y). \tag{5}$$

It can be seen in Fig. 7 that near the hh-lh crossover, the valence band at trap center is characterized by a shallow maximum near $k_{||} = 0$ (which becomes a stationary inflection point at the hh-lh crossover point), two maxima along the (110) direction, and two maxima along the $(1\bar{1}0)$ direction (these states are labeled A, B, and C, respectively). Due to symmetry, the two states corresponding to the "B" maxima will be identical and the two states corresponding to the "C" maxima will be identical. While all four critical points will have the same energy maximum and effective mass at trap center, away from the center along the [110] spatial direction the two B states will be slightly higher energy than the two C states. Meanwhile, the central valence band maximum (A) is pushed to higher energy

away from trap center until it becomes the global maximum and the transition once again becomes direct.

The asymmetry between the B and C states is caused by the presence of shear strain at the edges of the trap. Intuitively, at trap center one can see that the (110) and (1$\bar{1}$0) directions are identical, due to the symmetry of the trapping potential. Away from trap center along the [110] direction, there is an obvious asymmetry between the direction pointing directly towards/away from the center of the trapping potential (110) and the direction normal to it (1$\bar{1}$0).

A more quantitative explanation arises from the fact that the energy at finite k depends on a term proportional to $(k_x k_y)^2$. Away from trap center, there is a nonzero component of the strain that plays the same role, modifying this term into another of the form $(\frac{\hbar^2}{m_0}\sqrt{3}\gamma_3 k_x k_y - d\epsilon_{xy})^2$, where γ_3 is one of the Luttinger-Kohn parameters and d is a deformation potential parameter used in the Pikus-Bir Hamiltonian. This term breaks the degeneracy between the B and C states, depending on the sign of ϵ_{xy}, which is negative along the [110] axis and positive along the [1$\bar{1}$0] axis. For more details on the effect of finite in-plane k and strain on the interwell exciton energy, see Sinclair *et al.* [22] and Chuang's text [30].

The binding energy of an exciton is determined primarily by the reduced mass. This will be dominated by the much smaller electron mass, so it is reasonable to assume that it will not be drastically different for the five exciton states. Changing the exciton mass also alters the excitonic density of states, which also changes the recombination rate.

Given the effective mass of an exciton with spin degeneracy g_0, we can calculate the exciton density of states using the standard two-dimensional density of states [36],

$$\frac{g(\epsilon)}{A} = g_0 \frac{\bar{m}_{\mathrm{ex}}}{\pi \hbar^2}, \tag{6}$$

where $\bar{m}_{\mathrm{ex}}$ is the geometric mean of the effective mass along the two principal axes:

$$\bar{m}_{\mathrm{ex}} = \sqrt{m_{\mathrm{ex},110} m_{\mathrm{ex},1\bar{1}0}}. \tag{7}$$

The total number of excitons can then be calculated by summing the expected number of excitons in each state, assuming a Boltzmann distribution:

$$\begin{aligned} N_A &= e^{\mu/k_B T} \int_{E_0^{(A)}}^{E_0^{(A)}+\Delta E^{(A)}} g_A(\epsilon) e^{-\epsilon/k_B T} d\epsilon, \\ N_B &= 2e^{\mu/k_B T} \int_{E_0^{(B)}}^{E_0^{(B)}+\Delta E^{(B)}} g_B(\epsilon) e^{-\epsilon/k_B T} d\epsilon, \\ N_C &= 2e^{\mu/k_B T} \int_{E_0^{(C)}}^{E_0^{(C)}+\Delta E^{(C)}} g_C(\epsilon) e^{-\epsilon/k_B T} d\epsilon. \end{aligned} \tag{8}$$

In (8), the degeneracy of each state (g_0) is assumed to be the same. In this approximation, the slight valence band splitting at finite $k_{||}$ due to the presence of the electric field (visible in Fig. 8) is ignored. An upper energy cutoff (at $E_0 + \Delta E$) is used for each state to account for the regime where a maximum is present in the dispersion curve, but is shallow compared to $k_B T$. The number of excitons associated with the "A" valence band maximum, ignoring multiplicative constants common to N_A, N_B, and N_C, is

$$N_{\mathrm{A}} \propto k_B T \left[\bar{m}_{\mathrm{ex}}^{(A)} e^{-E_0^{(A)}/k_B T}\left(1 - e^{-\Delta E^{(A)}/k_B T}\right)\right]. \tag{9}$$

The result for the other B and C states will be similar to (9), replacing only the appropriate energy and effective mass parameters.

The external light cone is defined by the region of k space wherein an exciton can spontaneously decay into a photon outside of the sample (assuming an external index of refraction of unity). For this to be possible, conservation of in-plane momentum ($k_{||}$) and energy implies

$$\hbar c \sqrt{k_{z,\mathrm{ph}}^2 + k_{||}^2} = E_{\mathrm{ex}}(0) + \frac{\hbar^2 k_{||}^2}{2m_{\mathrm{ex}}}, \tag{10}$$

where $E_{\mathrm{ex}}(0)$ is the exciton energy at zero in-plane momentum. In this system, the dispersion relationship of the photon will be much sharper than that of the exciton, so only excitons near zero in-plane momentum will be able to recombine, and an even smaller fraction of these will reach the detector. The upper cutoff for the in-plane momentum of excitons which emit into the collection angle of the imaging optics (with numerical aperture NA) can approximately be reduced to the following inequality:

$$k_{||} \leqslant \mathrm{NA} \frac{E(k_{||} = 0)}{\hbar c}. \tag{11}$$

At zero strain, using the band gap of GaAs near absolute zero (1.52 eV) and an approximate confinement energy of 30 meV, the edge of the light cone outside the sample will occur around a $k_{||}$ value of 7.9 $\mu\mathrm{m}^{-1}$. The corresponding spread in energy associated with these states is on the order of a few μeV. The intensity that is actually observed at the ICCD will be a subset of this region of k space, limited by the numerical aperture of the collection optics (in the experiments described above, the numerical aperture was $\leqslant$0.5). If the radiative decay is slow enough for the exciton populations to remain near thermal equilibrium, the rate can be written in terms of the fraction of excitons capable of emitting photons within the collection angle, N_{obs}:

$$\frac{1}{\tau_{\mathrm{rad}}} \propto \frac{N_{\mathrm{obs}}}{N_A + 2N_B + 2N_C}. \tag{12}$$

The number of excitons observable by the ICCD (N_{obs}) can be found by integrating over the density of states in (8), within the k-space region bounded by (11). The range of energy associated with the external light cone is small compared to the thermal energy, $k_B T$, even at 1 K (83 μeV), and is even smaller within the region of k space that is optically accessible, making the k dependence of the integrand approximately constant. These two approximations greatly simplify the density of states integral, leaving an approximate expression for the temperature dependence of the number of excitons radiating into the collection angle of the imaging optics, N_{obs},

$$N_{\mathrm{obs}} \propto e^{-E_0^{(A)}/k_B T}. \tag{13}$$

Using this approximation with (12), which we will call the "exciton model," it is possible to calculate the detectable radiative rate as a function of position within the trapping potential. This is done by calculating the effective mass and

ground state energy associated with each exciton state (A, B, and C) based on the strain components at each point in the trap. This calculation was performed along a cross section on the [110] axis under the same conditions associated with Fig. 9(b). The detectable radiative rate [37] as a function of position is plotted in Fig. 9(a). To provide a fair comparison with the gap model, the rate is normalized in such a way that it approaches unity far from trap center.

This new rate is used to plot the intensity as a function of position in Fig. 9(c), which can be compared directly to the simpler model in Fig. 9(b) and the experimental series in Fig. 4. As seen in Fig. 9(a), the exciton model predicts a more gradual spatial dependence of the detectable radiative rate, due to the fact that it takes into account the effect of the variation of the in-plane effective mass on the fraction of excitons within the light cone, even in the direct regime. In Fig. 9(c), this results in a more rounded appearance to the intensity peaks at the edges of the dark spot and results in a distinct growth of this region with increased total density.

As noted above, the appearance of the momentum-space indirect gap requires that the radiative decay of the excitons not be governed by a single exponential rate across the entire trap. When the above mass-dependent effects are taken into account, this model predicts that the population decay can be calculated as a continuous superposition of exponentials, using the local lifetime for each position weighted by the density as a function of time. For a sufficiently sharp boundary between the bright and dark regions, this behavior can be approximated using a short-lifetime component associated with the bright region and a long-lifetime component associated with the dark region (which matches the experimentally observed behavior in Fig. 5).

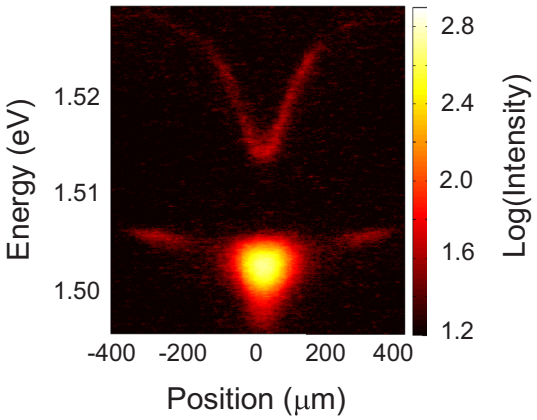

FIG. 10. (Color online) A spatial cross section of the spectrally resolved photoluminescence from a 12-nm CQW sample through trap center, in the high-stress regime where the light-hole luminescence is visible at trap center. Shown are the luminescence from intrawell excitons (the upper spectral line) and interwell excitons (the lower spectral line). In the interwell luminescence, one can see both the bright reappearing luminescence at trap center (associated with the reappearance of the direct radiative transition at high stress) and the region of suppressed luminescence surrounding the bright center. At higher stress, a larger region of the trap is pushed back into the direct-transition regime. At lower stress, the central region becomes dark again when it returns to the indirect-transition regime, discussed at length in previous sections. Data originally presented in Sinclair *et al.* [22].

V. REAPPEARANCE OF THE DIRECT GROUND STATE

As predicted by the model discussed in Sec. III, at high stress there is a reappearance of a momentum-space direct ground state at trap center, associated with the lh valence band crossing over the hh valence band. This was observed experimentally, with the appearance of a bright spot at the center of the trap at high stress. This feature, originally reported in Sinclair *et al.* [22] and shown here in Fig. 10, appears at higher stress than the dark spot onset and—as would be expected—occurs in a regime where the dark spot is still visible away from trap center.

To examine the central luminescence spot for the possibility of BEC, an optical coherence measurement was performed for 12-nm quantum wells [34], at low temperature (2.9 K) in the stress-regime where an approximately 50 μm diameter bright spot is visible at trap center (and the surrounding region is the dark spot regime).

The experiment was performed in a continuous flow cryostat with a collection angle of approximately 18° with respect to the sample normal. A Michelson interferometer was constructed with a plate beamsplitter and two, 3-inch diameter, front-surface mirrors. The overlapped image was focused onto the spectrometer slit with a spatial magnification on the CCD of 2.2 μm/pixel [the resulting photoluminescence image is shown in Fig. 11(a)]. Due to the long exposure time required to observe the interwell exciton luminescence, a reference He-Ne beam was used in conjunction with a piezo-driven active stabilization system to maintain a constant path length difference over the integration time (resulting in a phase stabilization of ±3°).

In this interference measurement, a spatial offset is introduced to the images in the two interferometer arms, caused by a small angular offset in the two mirrors. This additionally introduces an angular misalignment between the two rays, which will create fringing in a system with spatial coherence. A spatial offset of 12 μm was introduced between the two images and the resulting intensity (I_{1+2}) was compared to the intensity of the images with each individual interference arm blocked ($I_1 + I_2$). As shown in Fig. 11(b), the ratio of the overlapped intensity to the sum of the individual intensities did not reveal a distinguishable deviation from unity (apart from noise), indicating no measurable fringing. This indicates that the spatial coherence of the luminescence, if present, is less than the offset distance, 12 μm. A measurement of a smaller coherence length is limited by the size of the re-appearing luminescence at trap center and the resolution of the optical setup.

It is worth noting that the classical coherence length at this temperature is expected to be less than 100 nm, so this measurement does not necessarily exclude the possibility of a coherence length that is outside of the classical regime, but is less than 12 μm. It also does not eliminate the possibility of coherence in the optically forbidden spin states.

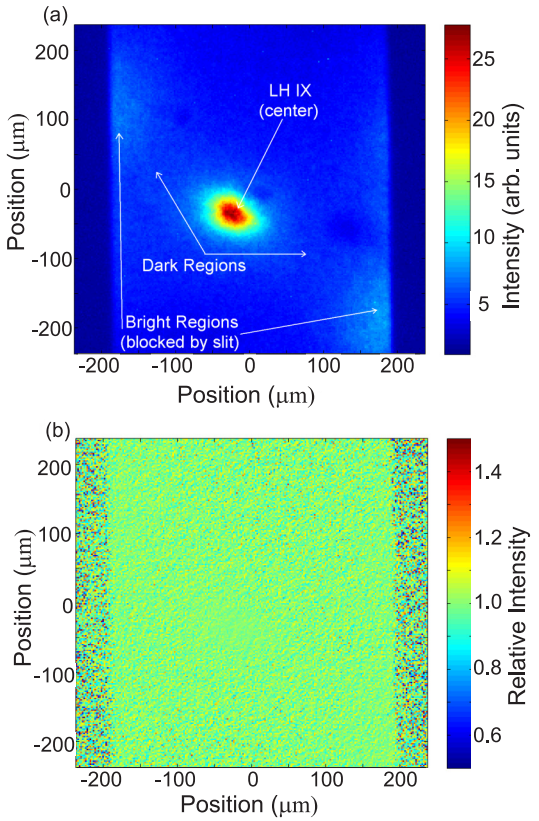

FIG. 11. (Color online) A 2D image of the IX photoluminescence intensity from a 12-nm CQW sample in the high-stress regime where the light-hole luminescence is visible at trap center. In (a), the intensity as a function of position on the sample is shown. The photoluminescence was sent through a Michelson interferometer with a small-angle offset in one mirror, resulting in a 12-μm spatial offset between the images at the detector. The intensity caused by the interference of the two images was normalized by the sum of the intensity values at each point for both individual images; this result is shown in (b). No detectable fringing is observed in (b), indicating a spatial coherence length of less than 12 μm.

VI. DISCUSSION

A model proposing an enhanced radiative rate on the sides of the trap was originally presented in Sinclair *et al.* [22] as one possible explanation for the darkening effect, with the caveat that many of the experimental features were not explained by the model, e.g., the temperature dependence, the fact that the modeled degree of darkening was not as significant as was observed, and the variation of the population lifetime with strain. In that analysis, it was suggested that the dark spot may appear because of radiative enhancement due to the light-hole fraction in conjunction with some other effect, such as an electron-hole liquid phase transition.

In this work, we have shown that the applied stress results in a slightly indirect band gap in the same stress regime where suppressed luminescence was previously reported. This implies the presence of both indirect-gap and direct-gap excitons, with virtually all light emission occurring from the direct-gap states. The two populations are expected to be in thermal equilibrium, with the lower-energy indirect states being primarily populated at low temperature. A simple model was proposed to connect this transition to photoluminescence measurements and was used to predict the variation of the photoluminescence profile with temperature, density, and stress. Qualitatively comparing these profiles to the experimental observations, it appears that the transition to an indirect band gap ties together all of the experimentally observed features of this effect.

Where does it leave this system in the search for Bose-Einstein condensation of indirect excitons? The suppression of direct band gap emission at trap center is problematic if optical measurements are the primary tool of investigations. Even if the direct transition is thermally allowed, the ground state of the system, which is momentum-space indirect, may not be optically accessible in the BEC regime. Still, it is worth remembering that one reason indirect excitons are a desirable system in the search for BEC is that they have a long radiative lifetime. If this effect is now understood, this method could provide an additional tool for enhancing the radiative lifetime of indirect excitons. Furthermore, the interaction between the hh-lh bands could open the door to experiments that are not possible with other trapping techniques.

The darkening at trap center can be avoided entirely by switching to narrower quantum wells, which would prevent the lh-hh crossing from occurring until much higher applied stresses. Narrow quantum wells generally have much more disorder, however [38], making spatial equilibrium more difficult to achieve. In principle, a very high quality narrow quantum well could allow a deep stress trap without a momentum-space direct-indirect crossover.

Alternatively, other types of nonoptical measurements can be used to explore BEC effects in this type of system. Bilayer exciton transport measurements in similar structures, with a permanent population due to doping, have shown evidence of coherence at low temperature and high magnetic field [39]. Similar experiments could be pursued in these structures, which have greater resemblance to a strongly interacting, but dilute, boson gas.

ACKNOWLEDGMENTS

This work was supported by the US Department of Energy, Grant No. DE-FG02-99ER457080. The work at Princeton University was funded by the Gordon and Betty Moore Foundation through the EPiQS initiative Grant No. GBMF4420, and by the National Science Foundation MRSEC Grant No. DMR-1420541.

[1] R. Balili, V. Hartwell, D. Snoke, L. Pfeiffer, and K. West, Science **316**, 1007 (2007).

[2] H. Deng, G. S. Solomon, R. Hey, K. H. Ploog, and Y. Yamamoto, Phys. Rev. Lett. **99**, 126403 (2007).

[3] C. W. Lai, N. Y. Kim, S. Utsunomiya, G. Roumpos, H. Deng, M. D. Fraser, T. Byrnes, P. Recher, N. Kumada, T. Fujisawa, *et al.*, Nature (London) **450**, 529 (2007).
[4] H. J. Polland, L. Schultheis, J. Kuhl, E. O. Göbel, and C. W. Tu, Phys. Rev. Lett. **55**, 2610 (1985).
[5] Z. Vörös, D. W. Snoke, L. Pfeiffer, and K. West, Phys. Rev. Lett. **97**, 016803 (2006).
[6] R. Zimmermann and C. Schindler, Solid State Commun. **144**, 395 (2007).
[7] Z. Vörös, D. W. Snoke, L. Pfeiffer, and K. West, Phys. Rev. Lett. **103**, 016403 (2009).
[8] D. A. B. Miller, D. S. Chemla, T. C. Damen, A. C. Gossard, W. Wiegmann, T. H. Wood, and C. A. Burrus, Phys. Rev. Lett. **53**, 2173 (1984).
[9] R. Rapaport, G. Chen, S. Simon, O. Mitrofanov, L. Pfeiffer, and P. M. Platzman, Phys. Rev. B **72**, 075428 (2005).
[10] A. Gärtner, D. Schuh, A. W. Holleitner, and J. P. Kotthaus, Physica E **40**, 1828 (2008).
[11] A. A. High, A. K. Thomas, G. Grosso, M. Remeika, A. T. Hammack, A. D. Meyertholen, M. M. Fogler, L. V. Butov, M. Hanson, and A. C. Gossard, Phys. Rev. Lett. **103**, 087403 (2009).
[12] A. A. High, J. R. Leonard, M. Remeika, L. V. Butov, M. Hanson, and A. C. Gossard, Nano Lett. **12**, 2605 (2012).
[13] A. A. High, J. R. Leonard, A. T. Hammack, M. M. Fogler, L. V. Butov, A. V. Kavokin, K. L. Campman, and A. C. Gossard, Nature (London) **483**, 584 (2012).
[14] M. Alloing, M. Beian, M. Lewenstein, D. Fuster, Y. González, L. González, R. Combescot, M. Combescot, and F. Dubin, Europhys. Lett. **107**, 10012 (2014).
[15] D. Semkat, S. Sobkowiak, G. Manzke, and H. Stolz, Nano Lett. **12**, 5055 (2012).
[16] J. Repp, G. J. Schinner, E. Schubert, A. K. Rai, D. Reuter, A. D. Wieck, U. Wurstbauer, J. P. Kotthaus, and A. W. Holleitner, Appl. Phys. Lett. **105**, 241101 (2014).
[17] R. S. Markiewicz, J. P. Wolfe, and C. D. Jeffries, Phys. Rev. B **15**, 1988 (1977).
[18] P. L. Gourley and J. P. Wolfe, Phys. Rev. B **20**, 3319 (1979).
[19] R. B. Balili, D. W. Snoke, L. Pfeiffer, and K. West, Appl. Phys. Lett. **88**, 031110 (2006).
[20] V. Negoita, D. W. Snoke, and K. Eberl, Appl. Phys. Lett. **75**, 2059 (1999).
[21] D. W. Snoke, Y. Liu, Z. Vörös, L. Pfeiffer, and K. West, Solid State Commun. **134**, 37 (2005).
[22] N. W. Sinclair, J. K. Wuenschell, Z. Vörös, B. Nelsen, D. W. Snoke, M. H. Szymanska, A. Chin, J. Keeling, L. N. Pfeiffer, and K. W. West, Phys. Rev. B **83**, 245304 (2011).
[23] M. Combescot, O. Betbeder-Matibet, and R. Combescot, Phys. Rev. Lett. **99**, 176403 (2007).
[24] R. Combescot and M. Combescot, Phys. Rev. Lett. **109**, 026401 (2012).
[25] Y. Shilo, K. Cohen, B. Laikhtman, K. West, L. Pfeiffer, and R. Rapaport, Nat. Commun. **4**, 2335 (2013).
[26] L. V. Butov, A. V. Mintsev, Y. E. Lozovik, K. L. Campman, and A. C. Gossard, Phys. Rev. B **62**, 1548 (2000).
[27] The dark region at trap center is also clearly visible in spectrally resolved images of the IX luminescence without the filter, verifying that the luminescence in the central region is not simply being cut out by the bandpass filter.
[28] L. C. Andreani, A. Pasquarello, and F. Bassani, Phys. Rev. B **36**, 5887 (1987).
[29] P. K. Basu, *Theory of Optical Processes in Semiconductors: Bulk and Microstructures: Bulk and Microstructures*, Vol. 4 (Oxford University Press, Oxford, UK, 1997).
[30] S. L. Chuang, *Physics of Photonic Devices*, Wiley Series in Pure and Applied Optics (John Wiley & Sons, Hoboken, NJ, 2009).
[31] B. D. Malone and M. L. Cohen, J. Phys.: Condens. Matter **25**, 105503 (2013).
[32] C. Schindler and R. Zimmermann, Phys. Rev. B **78**, 045313 (2008).
[33] Z. Vörös, Interaction of excitons in two-dimensional potentials, Ph.D. thesis, University of Pittsburgh, 2008.
[34] N. Sinclair, Luminescence darkening of strain-trapped excitons in coupled quantum wells, Ph.D. thesis, University of Pittsburgh, 2014.
[35] Identical in the sense that they have the same binding energy and effective mass.
[36] D. W. Snoke, *Solid State Physics: Essential Concepts* (Addison-Wesley, San Francisco, 2009).
[37] The detectable radiative rate refers to the rate of emission of photons into the collection angle of the imaging optics and is proportional to the measured intensity. For a quantitative prediction for the exciton lifetime, the rate of emission into the full light cone (both inside and outside the sample) would need to be considered.
[38] Z. Vörös, R. Balili, D. W. Snoke, L. Pfeiffer, and K. West, Phys. Rev. Lett. **94**, 226401 (2005).
[39] J. P. Eisenstein and A. H. MacDonald, Nature (London) **432**, 691 (2004).